# Earth's Future

**Key Points:**
- We predicted and highlighted the risk of abrupt biodiversity loss in terrestrial vertebrate species driven by increasing aridity
- More than 24% of terrestrial assemblages will be exposed to unprecedented aridity, and 55.29% of species will experience local habitat loss
- Concurrent extremes of increasing aridity and rising temperature in Southeast Asia and Amazon rainforests may amplify exposure risks

**Author Contributions:**
**Conceptualization:** Xiaoping Liu, Xiaocong Xu, Xia Li
**Formal analysis:** Renyun Guo, Xiaocong Xu
**Funding acquisition:** Xiaoping Liu, Xiaocong Xu

# Future Increase in Aridity Drives Abrupt Biodiversity Loss Among Terrestrial Vertebrate Species

**Xiaoping Liu[1,2]** , **Renyun Guo[1]** , **Xiaocong Xu[1]** , **Qian Shi[1]** , **Xia Li[3]** , **Haipeng Yu[4,5]** , **Yu Ren[5]**, and **Jianping Huang[5]**

[1]Guangdong Key Laboratory for Urbanization and Geo-Simulation, School of Geography and Planning, Sun Yat-Sen University, Guangzhou, China, [2]Southern Marine Science and Engineering Guangdong Laboratory (Zhuhai), Zhuhai, China, [3]Key Lab of Geographic Information Science (Ministry of Education), School of Geographic Sciences, East China Normal University, Shanghai, China, [4]Key Laboratory of Land Surface Process and Climate Change in Cold and Arid Regions, Northwest Institute of Eco-Environment and Resources, Chinese Academy of Sciences, Lanzhou, China, [5]Key Laboratory for Semi-Arid Climate Change of the Ministry of Education, College of Atmospheric Sciences, Lanzhou University, Lanzhou, China

**Abstract** The planet is predicted to become drier because of accelerating global warming, increasing great challenges to the survival of terrestrial species. However, the understanding of when and where increasing aridity in the future will lead to abrupt biodiversity loss is still limited. Here, we predicted the spatiotemporal dynamics of future vertebrate biodiversity loss driven by increasing aridity at the assemblage scale under the scenario framework of the shared socio-economic pathways (SSPs) and representative concentration pathways (RCPs). The results show that, under the high-emissions scenario of SSP5-8.5, more than 24.19% of terrestrial assemblages are projected to have at least one vertebrate species exposed to unprecedented aridity conditions by 2100, leading to 55.29% of terrestrial vertebrate species experiencing local habitat loss. In addition, the mean magnitude of global exposure is expected to reach 17.47% by 2100. Within these assemblages, most species will be simultaneously exposed to unprecedented aridity conditions, with an average exposure abruptness of 78.00%, most of which will occur intensively after 2050. If we manage to reduce greenhouse gas emissions to the SSP1-2.6 (SSP2-4.5) scenario, the magnitude of exposure can significantly decrease to 7.35% (10.56%), and the onset of exposure can be delayed by 43 (30) years, averaging approximately 30% (14%) of vertebrate species from local habitat loss. Our findings also highlight that the concurrent extremes of increasing aridity and rising temperature in Southeast Asia and Amazon rainforests may amplify exposure risks, which can motivate decision-makers to respond early and effectively to mitigate abrupt ecological disruption.

**Plain Language Summary** The global land surface is predicted to become more drier in the future due to the accelerating global warming, which places great challenges on the survival of terrestrial species. In this paper, we predicted the future spatiotemporal dynamics of biodiversity loss of vertebrate species as a result of the increase in aridity, trying to understand when and where the increasing aridity will cause biodiversity loss intensively and lead to abrupt ecological disruption. We found that, under the high-emissions scenario (~4.4°C global temperature rise), more than 24.19% of global terrestrial assemblages are projected to have at least one vertebrate species exposed to aridity condition exceeding their niche, leading to the consequence that 55.29% of species will experience habitat loss. The exposure events within most terrestrial assemblages will occur simultaneously after 2050. If we manage to reduce emissions to the low (intermediate)-emissions scenario (~1.8°C and 2.7°C global temperature rise), the onset of exposure can be delay by 43 (30) years. Our findings also highlight that the concurrent extremes of increasing aridity and rising temperature in Southeast Asia and Amazon rainforests may amplify exposure risks, which can motivate decision-makers to respond early to mitigate abrupt ecological disruption.

## 1. Introduction

In recent decades, global terrestrial biodiversity has decreased (Díaz et al., 2019; IPBES, 2019) as a joint result of climate change (e.g., global warming and related extreme events) and human pressures (e.g., agriculture and forestry activities). Anthropogenic climate change will continue to increase over time and consequently threaten the sustainability of terrestrial ecosystems (Brondízio et al., 2019; Hooper et al., 2012). More importantly, it will likely be the major driver of future biodiversity loss (Bellard et al., 2012; Maclean & Wilson, 2011; Román-Palacios

**Methodology:** Xiaocong Xu
**Resources:** Haipeng Yu, Yu Ren, Jianping Huang
**Supervision:** Qian Shi, Xia Li
**Writing – original draft:** Renyun Guo, Xiaocong Xu
**Writing – review & editing:** Renyun Guo, Xiaocong Xu

& Wiens, 2020; Urban, 2015). If we continue the high-emissions pathway (representative concentration pathway [RCP] 8.5; 4.3°C temperature rise by 2100), the global extinction risks, that is, the proportion of global species becoming extinct, are predicted to not only increase but also accelerate from 2.8% at present to ∼16% at the end of the century because of the global temperature rise (Urban, 2015).

Although numerous studies have been on biodiversity loss projections threatened by future climate change (Deutsch et al., 2008; Li et al., 2013; Román-Palacios & Wiens, 2020), most have focused on threats caused by changes in temperature and precipitation. By using species distribution models and future climate predictions, a series of studies have predicted the future survival of species in the warming future based on the concept of species climate niche (Colwell & Rangel, 2009; Elith & Leathwick, 2009; Elith et al., 2006; Marmion et al., 2009). For example, Trisos et al. (2020) projected and highlighted the impending risk of sudden and severe biodiversity loss because of future temperature rise and precipitation shifts. Indeed, changes in temperature and precipitation in the future will lead to a shift in new aridity patterns, with considerable spatial heterogeneity (Pendergrass & Hartmann, 2014; Shi et al., 2021). This resulting increase in aridity conditions is expected to alter ecosystem dynamics and various biogeochemical cycles (e.g., nutrient cycling and plant productivity; Delgado-Baquerizo et al., 2013; C. Wang et al., 2014), which will consequently lead to complicated biological consequences and pose great challenges to the survival of terrestrial species (Berdugo et al., 2020; Maestre et al., 2016). This situation is true even for humid and moist tropical regions because water availability and evapotranspiration are usually not uniformly distributed in the temporal dimension (Shi et al., 2021). Previous studies have suggested that even small changes in the dry season length can increase tree mortality rates in moist tropical forests (McDowell et al., 2018). Moreover, consistently longer dry seasons degrade tropical forest canopies (Brawn et al., 2017), decrease tropical bird population growth rates (Hilker et al., 2014), and have overwhelmingly detrimental effects and dire consequences for tropical biodiversity (Aguirre-Gutierrez et al., 2020; Gibson et al., 2011). Aridity is a synthetic indicator that combines information on multiple climate variables, including temperature, precipitation, specific humidity, and wind speed. Thus, the change in aridity is likely more biologically relevant. Assessing future biodiversity threatened by aridity increases is expected to reveal more comprehensive exposure information than considering temperature and precipitation separately. According to a global field survey analysis, there is a strong negative correlation between aridity and species richness in drier areas (García-Palacios et al., 2018), and aridity is considered one of the main reasons for the extinction of many species in Australia (Prideaux et al., 2009).

Recent research has shown that continuing warming will accelerate the increase in aridity worldwide (Berg et al., 2016; Feng & Fu, 2013; X. Wang et al., 2021). The dryland, defined as areas with rainfall less than 65% of evaporative demand (Delgado-Baquerizo et al., 2013), is projected to expand and cover more than 55% of the land surface by the end of the century under the RCP8.5 scenario (Huang et al., 2016). However, how and when terrestrial biodiversity will respond to increases in aridity under future warming scenarios remains to be elucidated. Furthermore, hazards that occur simultaneously in the same assemblage or a temporal sequence, such as heat extremes and drought events, may amplify exposure risks and lead to more compounded extinction (Masson-Delmotte et al., 2021). This is particularly true for species sensitive to temperature and water availability, such as amphibians and reptiles (Warren et al., 2013, 2018).

It is worth mentioning that, with limited exceptions (Trisos et al., 2020), most of the existing studies on biodiversity loss projection have mainly focused on spatial patterns at a snapshot of the future, typically at the end of the 21st century (Newbold, 2018; Warren et al., 2013, 2018). Although these snapshots describe the future spatial patterns of species at that specific time, they cannot account for the spatiotemporal dynamics of biodiversity disruption driven by climate change. Indeed, predicting and understanding these spatiotemporal dynamics will help us prepare for, and hopefully postpone, biodiversity loss and buy valuable time for species to adapt to future accelerating aridity (Bay et al., 2017). As for decision-makers, understanding how biodiversity gradually or suddenly changes from a temporal perspective (e.g., annual or decadal basis) will help them better assess biodiversity challenges and formulate conservation and emission reduction strategies. Most of the existing biodiversity loss predictions have been conducted at the species level, predicting the extinction probability of specific species threatened by climate change. However, predicting biodiversity loss by focusing on ecological assemblages is more informative for revealing how species respond to local climate change and the potential risk of abrupt ecological disruption.

This study focuses on the spatiotemporal dynamics of terrestrial vertebrate species responding to the future, increasing aridity at the ecological assemblage scale until the end of the century. To achieve this, we adopted an approach framework proposed by Trisos et al. (2020), combining the range of aridity niche limits of terrestrial

vertebrate species and future aridity projections under the scenario framework of the shared socio-economic pathways (SSPs) and RCPs, which was adopted in the Sixth Assessment Report (AR6) of the Intergovernmental Panel on Climate Change (IPCC). Specifically, we first calculated the time-series aridity index (AI) at the assemblage scale using the predicted climatic data of eight selected global climate models (GCMs) developed for the sixth phase of the Coupled Model Intercomparison Project (CMIP6) under three core sets of emission scenarios: SSP1-2.6, SSP2-4.5, and SSP5-8.5. We then assessed when and where terrestrial vertebrate species in ecological assemblages were locally exposed to aridity conditions beyond their niche limits. Finally, the cumulative percentage of species exposed over time within the assemblage, namely the horizon profile, was constructed to quantify the spatiotemporal risk of potential disruption of species in local assemblages driven by future aridity decline. Hopefully, these findings will deepen our understanding of the future spatiotemporal dynamics of terrestrial vertebrate species in response to dryer environments and motivate decision-makers to respond early and effectively to mitigate ecological disruption.

## 2. Materials and Methods

### 2.1. Terrestrial Biodiversity Data

The terrestrial vertebrate species data used in this study were acquired from the Red List of Threatened Species provided by the International Union for Conservation of Nature (IUCN) and Birdlife International (hereafter referred to as the IUCN Red List data set, https://www.iucnredlist.org/resources/spatial-data-download). The IUCN Red List data set is available in the Esri polygon shapefile format (organized in the WGS-1984 Geographic Coordinate System), describing the known spatial distributions of more than 105,500 species worldwide. These polygon maps are also known as extent-of-occurrence (EOO) maps (Joppa et al., 2016), typically hand-drawn by experts by applying a minimum convex polygon technique to "encompass all the known, inferred, or projected sites of present occurrence of a taxon, excluding cases of vagrancy." In this study, we focused on four clades of vertebrate species (~30,000 species): amphibians, mammals, birds, and reptiles (Table S1 in Supporting Information S1). According to the data guide of the IUCN Red List data set, the subsets of species labeled as critically endangered (CR), endangered (EN), and vulnerable (VU) were regarded as threatened groups in this study. These selected EOO polygon maps were then converted into equal-area grid cells at a spatial resolution of 100 km (Eckert IV projection), which is a reasonable scale globally without causing false species presence (Hurlbert & Jetz, 2007; Jetz et al., 2008). In this study, we defined species within an ecological assemblage (i.e., within a $100 \times 100$ km$^2$ grid cell) as local species, and multiple local species together form biological species globally.

### 2.2. Climate Model Data and Aridity Index

To derive the changes in future aridity conditions, we used climate simulations from eight selected GCMs (Table S2 in Supporting Information S1) of the latest CMIP6. We chose these GCMs according to the availability of climate data needed to calculate historical and future AI. For each GCM, we acquired time-series data of climate variables, including air temperature (°C), precipitation (mm), specific humidity (kg kg$^{-1}$), wind speed (m s$^{-1}$), surface air pressure (kPa), surface upward latent heat flux (W m$^{-2}$), and surface upward sensible heat flux (W m$^{-2}$) for the historical run of 1950–2014 and the future period of 2015–2100. Three illustrative SSP-RCP coupling scenarios, SSP1-2.6, SSP2-4.5, and SSP5-8.5, were chosen to cover the range of possible future developments of anthropogenic drivers of climate change (Masson-Delmotte et al., 2021; Tebaldi et al., 2021). The SSP1-2.6 refers to the combination of SSP1 and RCP 2.6, which represents the low greenhouse gas (GHG) emissions scenario with CO$_2$ emissions declining to net zero around or after 2050 and the global warming limited to 1.8°C (likely 1.3°C–2.4°C) by 2100 relative to 1850–1900 (IPCC, 2021). Similarly, the SSP2-4.5 is the intermediate GHG emissions scenario with CO$_2$ emissions remaining around current levels, and the temperature rise will be 2.7°C (likely 2.1°C–3.5°C); and the SSP5-8.5 represents the high GHG emissions scenario that roughly double the current emission levels by 2100, and the temperature rise is expected to be 4.4°C (likely 3.3°C–5.7°C).

The aridity condition of the land surface is meteorologically related to water availability (water supply and evaporative demand), and various techniques have been proposed to precisely define it (Stadler, 1998). The AI is one of the most commonly used indicators and is defined by the United Nations Environmental Programme (Middleton & Thomas, 1992) as the ratio of total precipitation (*P*) to total potential evapotranspiration (PET):

$$AI = \frac{P}{PET} \tag{1}$$

AI a is a nonnegative value, and a smaller AI value indicates drier conditions. It provides a reasonable proxy for the historical, current, and future projected ecohydrological states of the land surface with respect to long-term dryness (Greve et al., 2019; Xu et al., 2021). In recent decades, AI has become one of the most widely used quantitative indicators in the evaluation of dry climate conditions across different geographic areas of the world (Dave et al., 2019; Feng & Fu, 2013; Greve et al., 2019; Huang et al., 2016; Mortimore et al., 2009; Wen et al., 2018). Compared with other meteorological drought indices, such as the Palmer drought severity index and standardized precipitation evapotranspiration index, the AI is more suitable for the characterization of climatic drought conditions and the classification of climatic zones at local and global scales (Chai et al., 2021).

PET is a vital part of the AI, and the Food and Agriculture Organization (FAO) has recommended the Penman-Monteith (PM) method (Maidment, 1993; Penman, 1948) as the standard method for the estimation of PET with a series of climate variables, including radiation, heat flux, temperature, vapor pressure, and wind speed (Allen et al., 1998). However, the PM method does not consider the increase in surface resistance driven by rising $CO_2$ in the atmosphere, which will offset the increase in evapotranspiration caused by the increase in warming-induced vapor pressure deficit and consequently result in the overestimation of future drying trends (Aadhar & Mishra, 2019, 2020; Milly & Dunne, 2016; Swann et al., 2016). Thus, in this study, we adopted the modified PM method proposed by Yang et al. (2019) to avoid the bias caused by future climate warming.

$$\text{PET} = \frac{0.408\Delta(R_n - G) + \gamma \frac{900}{T+273} u_2 (e_s - e_a)}{\Delta + \gamma \left\{ 1 + u_2 \left[ 0.34 + 2.4 \times 10^{-4}([CO_2] - 300) \right] \right\}} \tag{2}$$

where $\Delta$ denotes the slope of the change in the saturation vapor pressure in relation to air temperature (kPa °C$^{-1}$); $R_n$ and $G$ denote the net radiation at the canopy surface and soil heat flux density (MJ m$^{-2}$ day$^{-1}$), respectively; $\gamma$ is a psychrometric constant (kPa °C$^{-1}$); $T$ denotes the mean daily air temperature at 2 m height (°C); $u_2$ denotes the wind speed at 2 m (m s$^{-1}$); $e_s$ and $e_a$ are the saturation vapor pressure and actual vapor pressure (kPa), respectively; and $\left[ 0.34 + 2.4 \times 10^{-4}([CO_2] - 300) \right]$ accounts for the surface resistance driven by rising $CO_2$ in the atmosphere (Yang et al., 2019). The time-series PET values of each grid were calculated according to Equation 2 using climate data from eight CMIP6-GCMs (Table S2 in Supporting Information S1) and $CO_2$ concentration data from the data set developed by Meinshausen et al. (2017, 2020). To prevent interference from extreme PET outliers, we fixed the PET values that exceed 1.5 times the interquartile range outside the 25th (first quartile) and 75th percentiles (third quartile) of the time-series PET sequence:

$$\text{PET}_t^i = \begin{cases} Q_3^i + 1.5 \times \text{IQR}^i & \text{if PET}_t^i \geq Q_3^i + 1.5 \times \text{IQR}^i \\ Q_1^i - 1.5 \times \text{IQR}^i & \text{if PET}_t^i \leq Q_1^i - 1.5 \times \text{IQR}^i \\ \text{PET}_t^i & \text{else} \end{cases} \tag{3}$$

where $\text{PET}_t^i$ is the PET value in year $t$ for grid $i$; $Q_1^i$ and $Q_3^i$ are the 25th and 75th quartiles of the time-series PET sequence for grid $i$, respectively; and $\text{IQR}^i$ is the interquartile range of the time-series PET sequence for site $i$. Extreme outlier removal, in this manner, follows the rules of removing extreme outliers in the construction of the box plot. This method is more robust for PET and AI because it does not require data to have a Gaussian distribution. We also conducted the same procedure for $P$ to remove outliers from the time-series precipitation. Instead of using the ensemble mean of multiple GCMs, we calculated the values of AI according to Equation 1 for each assemblage using climate simulation from each GCM to maintain the internal variance in the time series. Given that CMIP6 models use different sizes of spatial grids, we interpolated and regridded the AI maps into 100 km grid cells to match the spatial resolution of species geographic range data. Dryland areas are defined as regions where AI < 0.65 and are further divided into four subtypes: hyperarid (AI < 0.05), arid ($0.05 \leq$ AI < 0.2), semiarid ($0.2 \leq$ AI < 0.5), and dry subhumid ($0.5 \leq$ AI < 0.65).

## 2.3. Projection of Future Biodiversity Threat

### 2.3.1. Determination of Species-Realized Aridity Limits

In our study, we defined the timing of aridity exposure for local species as the year in the future, after which the aridity condition within the ecological assemblage consistently exceeded the aridity limit a species can endure.

Thus, the aridity limit for each species should be determined beforehand. Note that exposure to a dryer environment beyond the species' realized niche does not necessarily equate to local extinction but provides a precautionary warning for biodiversity risk (Colwell et al., 2008; Scheffer et al., 2009; Warren et al., 2018). The niche limits of species are typically related to climate change in space and time dimensions. Unlike previous studies that used time-averaged climate conditions (Hijmans et al., 2005), we followed the framework of Trisos et al. (2020), incorporating the temporal and spatial variabilities of aridity conditions to determine the species-realized aridity limits from the historical run of the AI estimates (1950–2014).

First, for each ecological assemblage, the local aridity limit was determined by the minimum value (i.e., the driest condition) from the time-series AI sequence from 1950 to 2014. The variables used to calculate the time-series AI values, including air temperature, precipitation, specific humidity, wind speed, surface air pressure, surface upward latent heat flux, and sensible heat flux were derived from eight CMIP6-GCMs. These time-series projections from individual GCMs during the historical period involve biases and extreme outlier values beyond a reasonable range, particularly for the precipitation variable. Without proper removal of these extreme outliers, these biases and extreme values will result in unstable time-series AI calculations and consequently cause biases in estimating species aridity niches. To prevent interference from extreme AI outliers, we excluded values that exceed 1.5 times the interquartile range outside the 25th and 75th percentiles of the time-series AI sequence. Thus, the local aridity limit of a site can be mathematically expressed as follows:

$$\mathrm{LAL}^i = \min\left\{\mathrm{AI}^i_t \big| Q^i_1 - 1.5 \times \mathrm{IQR}^i \leq \mathrm{AI}^i_t \leq Q^i_3 + 1.5 \times \mathrm{IQR}^i\right\}$$
$$\mathrm{IQR}^i = Q^i_3 - Q^i_1 \tag{4}$$

where $\mathrm{LAL}^i$ denotes the local aridity limit for site $i$; $\mathrm{AI}^i_t$ is the time-series AI value for site $i$ in year $t$; $Q^i_1$ and $Q^i_3$ are the 25th and 75th quartiles of the time-series AI sequence for site $i$, respectively; and $\mathrm{IQR}^i$ is the interquartile range of the time-series AI sequence for site $i$.

Second, for each species, the species-realized aridity limit was determined by overlapping the IUCN EOO map with the derived local aridity limits from Equation 4. Specifically, the species-realized aridity limit was determined as the minimum value of the local aridity limits across all ecological assemblages where the target species occurred. To avoid extreme outliers from some ecological assemblages calculated by climate variables from individual GCM, extreme outliers were excluded using the same method as in Equation 4, as follows:

$$\mathrm{SRAL}^s = \min\left\{\mathrm{LAL}^{i,s}_k \big| Q^s_1 - 1.5 \times \mathrm{IQR}^s \leq \mathrm{LAL}^{i,s}_k \leq Q^s_3 + 1.5 \times \mathrm{IQR}^s\right\}$$
$$\mathrm{LAL}^{i,s} = \left\{\mathrm{LAL}^i \big| \mathrm{occured}^{i,s} = 1\right\} \tag{5}$$
$$\mathrm{IQR}^s = Q^s_3 - Q^s_1$$

where $\mathrm{SRAL}^s$ denotes the determined species-realized aridity limit for species $s$; $\mathrm{LAL}^{i,s}$ is a subset of $\mathrm{LAL}^i$ in Equation 4 under the condition where species $s$ was reported in ecological assemblages $i$ according to the IUCN EOO maps; $\mathrm{occured}^{i,s}$ is a Boolean value indicating whether species $s$ exists (i.e., 1) in ecological assemblages $i$ or not (i.e., 0); $\mathrm{LAL}^{i,s}_k$ is the $k$th element of the $\mathrm{LAL}^{i,s}$ sequence; $Q^s_1$ and $Q^s_3$ are the 25th and 75th quartiles of the $\mathrm{LAL}^{i,s}$ sequence, respectively; $\mathrm{IQR}^s$ is the interquartile range of the $\mathrm{LAL}^{i,s}$ sequence.

### 2.3.2. Determination of Local Species Exposure Timing

For each terrestrial assemblage, the timing for a local species exposed to aridity was determined as the year after which the future AI is projected to be smaller than the derived species-realized aridity limit for at least five consecutive years, which can be expressed as

$$T^{i,s}_{\mathrm{exposed}} = \begin{cases} \min(t) + 5 & \mathrm{AI}^i_{t+k} < \mathrm{SRAL}^s, \forall k \in \{0, 1, 2, 3, 4\} \\ \infty & \mathrm{others} \end{cases} \tag{6}$$

where $T^{i,s}_{\mathrm{exposed}}$ denotes the exposure time of local species $s$ located in ecological assemblage $i$; $\mathrm{SRAL}^s$ is the species-realized aridity limit for species $s$ derived from Equation 5; $\mathrm{AI}^i_{t+k}$ is the projected AI value in future year $t + k$ for ecological assemblage $i$; $k$ is a consecutive year duration. We were aware that the consecutive

duration of exposure to aridity that leads to local population decline and even extinction is still unclear and may vary across different species and geographical regions. Nevertheless, exposure to aridity for five consecutive years can still severely impact the survival of most annually bred species. A previous study also showed that using an interval longer than five consecutive years had little effect on quantifying exposure timing to extreme temperature and precipitation (Trisos et al., 2020). Thus, the consecutive year duration in this study was set to be 5 years. If the future AI sequence of an ecological assemblage was higher than the species-realized aridity limit until the end of the century, then there was no exposure for this ecological assemblage, and the timing of exposure was flagged to ∞.

### 2.3.3. Horizon Profile of Ecological Assemblages

When all local species exposure times were calculated for an ecological assemblage, we constructed a horizon profile to summarize the temporal dynamics of biodiversity exposure as a result of future increased aridity. In this study, the horizon profile of an ecological assemblage was defined as a curve in which the time-series values denoted the cumulative percentage of species locally exposed to conditions beyond their realized aridity limits (the solid black curve in Figure S1 in Supporting Information S1). To construct the horizon profile, we first need to identify the exposure status of the ecological assemblage, that is, whether and when a local species exceeds its aridity limit in each year of the future study period:

$$\text{Exposed}_t^{i,s} = \begin{cases} 1 & t \geq T_{\text{exposed}}^{i,s} \\ 0 & \text{others} \end{cases} \tag{7}$$

where $\text{Exposed}_t^{i,s}$ denotes whether local species $s$ located in ecological assemblage $i$ will experience exposure events in future year $t$; and $T_{\text{exposed}}^{i,s}$ is the timing of exposure for local species $s$ located in ecological assemblage $i$. Note that if a local species is identified as being exposed in future year $t$, this status will persist afterward until the end of the century. Based on the exposure status for each ecological assemblage $i$, we calculated the cumulative percentage of exposure for each year, that is, the ratio of exposed local species to all local species by that year, as follows:

$$\text{CPE}_t^i = \frac{1}{N^i} \sum_{s=1}^{N^i} \text{Exposed}_t^{i,s} \tag{8}$$

where $\text{CPE}_t^i$ denotes the cumulative percentage of exposure (hereafter referred to as CPE) for ecological assemblage $i$ in future year $t$, $\text{Exposed}_t^{i,s}$ is the exposure status defined in Equation 7, and $N^i$ is the number of local species populated in ecological assemblage $i$.

Note that the horizon profile can also be constructed for regional and global scales, that is, a biome or the entire terrestrial biosphere regarding the research scales. Thus, we aggregated all terrestrial assemblages and estimated the global horizon profile to describe the overall temporal dynamics of the cumulative exposure for all terrestrial vertebrate species. To prevent the derived temporal dynamics from being dominated by some widely distributed species, we weighted each species with the inverse of its spatial distribution range: the total number of ecological assemblages where the species occurred. All species contributed equally to the derived aggregated temporal exposure dynamics through this weighting. To avoid confusion, we refer to this aggregated regional or global horizon profile as the mean percentage of geographic range exposure (MPGE):

$$\text{MPGE}_t = \frac{1}{N^s} \sum_{s=1}^{N^s} \left( \frac{1}{r_s} \sum_{i=1}^{N^a} \text{Exposed}_t^{i,s} \right) \tag{9}$$

where $\text{MPGE}_t$ denotes the MPGE in future year $t$; $r_s$ is the spatial distribution range of species $s$, that is, the total number of ecological assemblages where the species $s$ occurred; $N^a$ is the total number of ecological assemblages in the study region; and $N^s$ is the number of species within the study region.

All ecological assemblages within a species' geographic distribution in the IUCN EOO map were considered habitats. Suppose the future aridity condition in ecological assemblages exceeds the realized aridity limit of a species for at least five consecutive years. In that case, these assemblages are no longer suitable for this species

and are therefore regarded as a loss of habitat for this species locally after this time. Thus, from the species' perspective, the percentage of geographic exposure (PGE) indicator for a specific species can be defined to quantify the local habitat loss of species because of unprecedented aridity conditions as follows:

$$\text{PGE}_t^s = \frac{1}{r_s} \sum_{i=1}^{N^a} \text{Exposed}_t^{i,s} \tag{10}$$

where $\text{PGE}_t^s$ denotes the percentage of geographic range exposure for species $s$ in future year $t$. The other notations are identical to those used in Equation 9.

### 2.3.4. Feature Indicators of Horizon Profile

Based on the above-defined horizon profiles (for ecological assemblage or regional aggregation), we used the following indicators to quantify the future spatiotemporal exposure dynamics of terrestrial vertebrate species to unprecedented accelerating aridity. First, for each ecological assemblage, we estimated the percentage of local species that would be exposed to aridity until the end of the century as the magnitude of local exposure, which is equivalent to the cumulative percentage of local exposure in 2100, as follows:

$$\text{EM}^i = \text{CPE}_{2100}^i \tag{11}$$

Additionally, the cumulative number of local exposures for each ecological assemblage by the end of the century is estimated as follows:

$$\text{EN}^i = \sum_{s=1}^{N^i} \text{Exposed}_{2100}^{i,s} = N^i \times \text{CPE}_{2100}^i \tag{12}$$

where $N^i$ is the number of local species in the ecological assemblage $i$. We used a moving window to calculate the difference in CPE within each 10-year interval and extracted its maximum as the decadal maximum exposure for an ecological assemblage. Then, we defined the abruptness of local exposure as the proportion of decadal maximum exposure to all local exposures (the species exposure covered by the shaded areas of 10-year interval in Figure S1 in Supporting Information S1), as follows:

$$\text{EA}^i = \frac{\max\left\{\text{CPE}_{t+10}^i - \text{CPE}_t^i\right\}}{\text{EM}^i} \tag{13}$$

Note that abruptness of exposure was only calculated for ecological assemblages within which five or more local species were identified as exposed to aridity. Finally, we excluded local species that would not be exposed and defined the timing of local exposure as the median of the exposure timings for the rest of the local species within the ecological assemblage (the year indicated by the arrow in Figure S1 in Supporting Information S1), as follows:

$$\text{ET}^i = \text{median}\left\{T_{\text{exposed}}^{i,s} \,|\, T_{\text{exposed}}^{i,s} \neq \infty\right\} \tag{14}$$

We also excluded ecological assemblages with fewer than five local species exposed to aridity to avoid uncertainties caused by the small sample size. The timing of local exposure can also be alternatively determined by the mean year of exposure and the midyear of the decade with the maximum exposure. These four indicators, magnitude, number, abruptness, and timing of local exposure, describe the shape of the horizon profile from different dimensions. The magnitude and number focus on the percentage and number of locally exposed species, whereas the abruptness describes the synchronicity in the timing of exposure and the timing emphasizes the median year for local species exposed to unprecedented aridity. With the AI calculated for each assemblage from the eight GCMs separately, we estimated these four indicators for each GCM to maintain the internal variance in the time series. The exposure results were then summarized by averaging all results across individual GCMs to capture the uncertainty and void bias because of specific GCM simulations during the exposure assessments. Hopefully, biodiversity threats driven by future accelerated aridity and potential ecological disruption can be well described through these indicators.
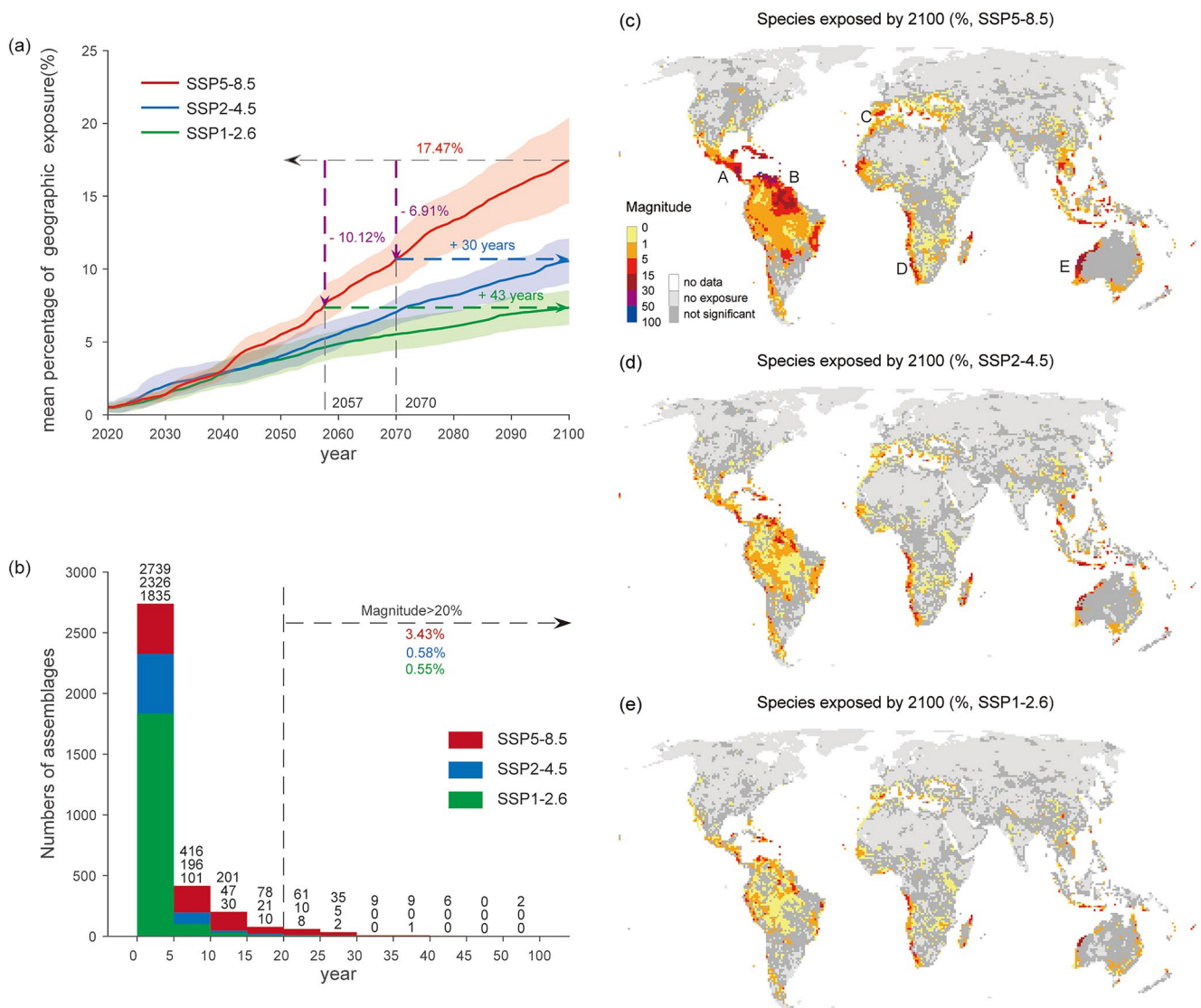
**Figure 1.** The global horizon profile of terrestrial vertebrate species under the SSP1-2.6, SSP2-4.5, and SSP5-8.5 scenarios. (a) The mean percentage of geographic range exposure (solid lines) before the end of the century. For each scenario, the 95% confidence intervals of eight global climate models (GCMs; shading areas) illustrate the variability in exposure across different GCMs. (b) Comparison of the histogram of CPE under three scenarios by 2100. (c) The magnitude of local exposure by 2100 under the SSP5-8.5 scenario. Hotspots of exposure are labeled as A–E. (d) Same as (c) but under the SSP2-4.5 scenario. (e) Same as (c) but under the SSP1-2.6 scenario.

## 3. Results

### 3.1. Horizon Profile Terrestrial Vertebrate Species

By combining the spatial distribution of terrestrial vertebrate species from the IUCN Red List data set and future aridity conditions calculated from eight CMIP6-GCMs, we estimated the future timing at which local terrestrial vertebrate species experience unprecedented aridity conditions that exceed their species-realized aridity limits under the SSP1-2.6, SSP2-4.5, and SSP5-8.5 scenarios. For each terrestrial assemblage, the cumulative percentage of local species exposed to aridity conditions was estimated for each GCM over the century. We further aggregated the horizon profiles of all terrestrial assemblages and constructed a global horizon profile, the MPGE, to present the overall exposure dynamics for terrestrial vertebrate species (Figure 1).

We found that, for all terrestrial vertebrate species, the MPGE to unprecedented aridity conditions will reach 17.47% by the end of this century under the high-emissions scenario of SSP5-8.5 (red line in Figure 1a). If we manage to reduce GHG emissions to the intermediate (SSP2-4.5) and low (SSP1-2.6) emission scenarios, the

MPGE will significantly decrease to 10.56% and 7.35% (the blue and green lines in Figure 1a) in 2100. These exposure levels are equivalent to those in the 2070s and the 2050s under the SSP5-8.5 scenario. Additionally, according to the projections, more than 24% (3,556 assemblages), 17% (2,605 assemblages), and 13% (1,987 assemblages) of terrestrial assemblages were projected to have at least one local species threatened by unprecedented aridity conditions by 2100 under scenarios SSP5-8.5, SSP2-4.5, and SSP1-2.6, respectively (Table S3 in Supporting Information S1). Most exposed assemblages were expected to encounter relatively low exposure (Figure 1b). For example, 88.72% (3,155 assemblages) of the exposed assemblages are projected to have a CPE of less than 10% under the SSP5-8.5 scenario (Table S3 in Supporting Information S1), equivalent to 21.46% of all terrestrial assemblages. Situations were much better under the intermediate- and low-concentration scenarios of SSP2-4.5 and SSP1-2.6, with 96.81% (2,522 assemblages) and 97.43% (1,936 assemblages) of exposed assemblages projected to have a CPE of less than 10%, equivalent to 17.16% and 13.17% of all terrestrial assemblages, respectively.

The magnitude of local exposure by 2100 was found to vary across terrestrial assemblages globally (Figures 1c–1e). Generally, the magnitude of exposure is projected to increase, and the spatial distribution will expand over time until the end of the century (Figure S2 in Supporting Information S1 for SSP5-8.5, Figure S3 in Supporting Information S1 for SSP2-4.5, and Figure S4 in Supporting Information S1 for SSP1-2.6). Regions of the southern Mexico (A in Figure 1c), the northern Amazon rainforest (B), the Iberian Peninsula (C), the west coast of Africa (D), and the west coast of Australia (E) are the hotspots of exposure, with local species in most assemblages exposed to unprecedented aridity conditions by 2100 under the SSP5-8.5 scenario (Figure 1c). Although the magnitudes of local exposure under the SSP2-4.5 and SSP1-2.6 scenarios are relatively smaller than those under the SSP5-8.5 scenario, their spatial patterns are quite similar (Figures 1d and 1e). According to previous studies, a 20% loss of local species is considered a safe limit, and a decline in species diversity exceeding this limit would result in serious consequences and even ecosystem collapse (Hooper et al., 2012; Newbold et al., 2016). Our results show that driven by unprecedented aridity conditions, 3.43% (122 assemblages) of exposed assemblages are expected to exceed this safe limit by 2100 under the SSP5-8.5 scenario (Figures 1b and 1c). Situations are much more promising under the intermediate- and low-concentration scenarios, with only 0.58% (15 assemblages) and 0.55% (11 assemblages) of exposed assemblages encountering local species loss exceeding 20%, most of which are located in regions of the southern Mexico, the northern part of the Amazon rainforest (Figures 1c–1e).

The physiological diversity of the four selected vertebrate clades, that is, amphibians, mammals, birds, and reptiles, could result in varying responses to future aridity conditions because they have different limits of the aridity niche. We constructed horizon profiles separately for the four clades and found that the exposed terrestrial assemblages were spatially consistent among the four clades under the three scenarios (Figures S5–S7 in Supporting Information S1). The results show that although the spatial ranges of exposed habitat for amphibian (2,050 assemblages, 16.44%) and reptile (2,093 assemblages, 16.39%) species are close to those of mammal (2,210 assemblages, 15.03%) and bird (1,988 assemblages, 13.54%) species, substantially higher MPGE was observed for amphibian (30.75%) and reptile (23.58%) species (Table S4 in Supporting Information S1), because a larger portion of their habitat assemblages is projected to have higher magnitude of exposure (Figures S5a–S5c and S5j–S5l in Supporting Information S1). Previous studies have pointed out that amphibians and reptiles are more sensitive to changes in climate and the environment (Newbold, 2018; Warren et al., 2013), and our results support this opinion from the aridity perspective. More attention is urgently needed to protect these most at-risk amphibian and reptile species, buying valuable time to adapt to a dryer environment and reduce the risk of ecological disruption.

From the species' perspective, we investigated the extent of local habitat loss because of future unprecedented aridity conditions (Table 1). Note that the extent of local habitat loss in this study refers to a reduction in the amount of living space owing to the future increase in aridity. It equals the percentage of ecological assemblages within which a species will be exposed to aridity conditions beyond its aridity niche. The results show that there will be 16,350 (55.29%) selected terrestrial vertebrate species (29,572 in total) experiencing local habitat loss by 2100 under the SSP5-8.5 scenario. More importantly, under this high-emissions scenario, 7.18% of selected terrestrial vertebrate species will undergo severe survival threats by 2100, and all their habitat assemblages are projected to be exposed to dryer environments than their species-realized aridity limits. In other words, their original habitats will not be suitable for these species by 2100 unless they adapt to a dryer environment or migrate to more humid regions. Among the four selected vertebrate clades, habitats of amphibian and reptile species faced

**Table 1**
*Number and Percentage of Terrestrial Species Undergoing Local Habitat Loss for Different PGEs by 2100*

| Percentage of geographic exposure (PGE) | SSP5-8.5 | | | SSP2-4.5 | | | SSP1-2.6 | | |
|---|---|---|---|---|---|---|---|---|---|
| | >0 | >50% | 100% | >0 | >50% | 100% | >0 | >50% | 100% |
| All terrestrial vertebrate | 16,350 | 4,896 | 2,122 | 12,191 | 2,550 | 1,387 | 7,441 | 1,366 | 899 |
| | 55.29% | 16.56% | 7.18% | 41.22% | 8.62% | 4.69% | 25.16% | 4.62% | 3.04% |
| Amphibian | 4,211 | 2,183 | 1,064 | 3,115 | 1,221 | 677 | 2,080 | 734 | 483 |
| | 64.15% | 33.26% | 16.21% | 47.46% | 18.60% | 10.31% | 31.69% | 11.18% | 7.36% |
| Mammal | 2,849 | 538 | 182 | 2,168 | 281 | 126 | 1,283 | 115 | 65 |
| | 50.29% | 9.50% | 3.21% | 38.27% | 4.96% | 2.22% | 22.65% | 2.03% | 1.15% |
| Bird | 5,483 | 556 | 137 | 4,092 | 214 | 101 | 2,417 | 74 | 52 |
| | 51.79% | 5.25% | 1.29% | 38.65% | 2.02% | 0.95% | 22.83% | 0.70% | 0.49% |
| Reptile | 3,807 | 1,619 | 739 | 2,816 | 834 | 483 | 1,661 | 443 | 299 |
| | 56.36% | 23.97% | 10.94% | 41.69% | 12.35% | 7.15% | 24.59% | 6.56% | 4.43% |

more severe threads under all emission scenarios. For example, 64.15% (4,211 out of 6,564) of amphibians and 56.36% (3,807 out of 6,755) of reptile species experienced at least one habitat assemblage loss by 2100 under the SSP5-8.5 scenario (Table 1). In addition, 16.21% (1,064 out of 6,564) of amphibians and 10.94% (739 out of 6,755) of reptile species will lose all their habitat assemblages by 2100. Local habitat loss is still a difficult challenge, even under intermediate- and low-emission scenarios. Projections show that there are 1,387 (4.69%) and 899 (3.04%) terrestrial vertebrate species facing a distinctive survival threat from unprecedented aridity conditions by 2100 under the SSP2-4.5 and SSP1-2.6 scenarios, with most of them being amphibian (677, 10.31%; 483, 7.36%) and reptile (483, 7.15%; 299, 4.43%) species.

### 3.2. Abruptness and Timing of Local Exposure

In addition to the magnitude of exposure, we further investigated other key features of the horizon profile better to understand the temporal dynamics of future biodiversity exposure. The most notable feature of the horizon profile for a local assemblage is its abruptness, which quantifies the synchronicity of the local exposure within a local assemblage. Higher abruptness warns of potential ecological disruption because the cooccurring species are likely to be exposed to dryer conditions simultaneously within a short period. Our projections showed that the spatial patterns and hotspots of the abruptness of exposure were geographically highly consistent with the magnitude of exposure (Figure 2). For all exposed terrestrial assemblages, an average level of 78.00% (median, and 77.78% for mean) of local exposure timings was projected to occur within a single decade under the SSP5-8.5 scenario (Figure 3). Additionally, the median of exposure abruptness for local assemblages was found to be synchronized among horizon profiles constructed from four clades separately within local assemblages (Table 2), with the median of exposure abruptness ranging from 76.48% to 80.70% (76.78%–80.56% for mean). Although the magnitude, extent, and number of exposure events were smaller under the SSP2-4.5 and SSP1-2.6 scenarios (Figure 1 and Figure S8 in Supporting Information S1), the average level of the abruptness of local exposure was found to be slightly higher (83.52% for median and 82.13% for mean under the SSP2-4.5 scenario; 87.07% for median and 84.41% for mean under the SSP1-2.6 scenario), revealing a relatively more synchronized pattern of these exposure events under the intermediate- and low-emissions scenarios. Notably, amphibians (86.74% and 92.31% for median) and reptile clades (90.56% and 94.44% for median) faced higher abruptness of exposure than species of mammals (85.42% and 87.50% for median) and bird clades (82.19% and 84.22% for median) under the SSP2-4.5 and SSP1-2.6 scenarios (Table 2).

Although the abruptness of exposure varies across different areas, assemblages with higher abruptness are primarily centered on regions with a higher magnitude of exposure, such as the southern Mexico and the northern part of the Amazon rainforest. This clustering pattern of abruptness may be partially explained by the fact that species living in adjacent assemblages often share similarly realized aridity. Moreover, we found that events of exposure with a higher magnitude were likely to occur more abruptly for local species. Such cooccurring exposure events within a short period among various local species could lead to devastating consequences for local biodiversity and ecosystem services.
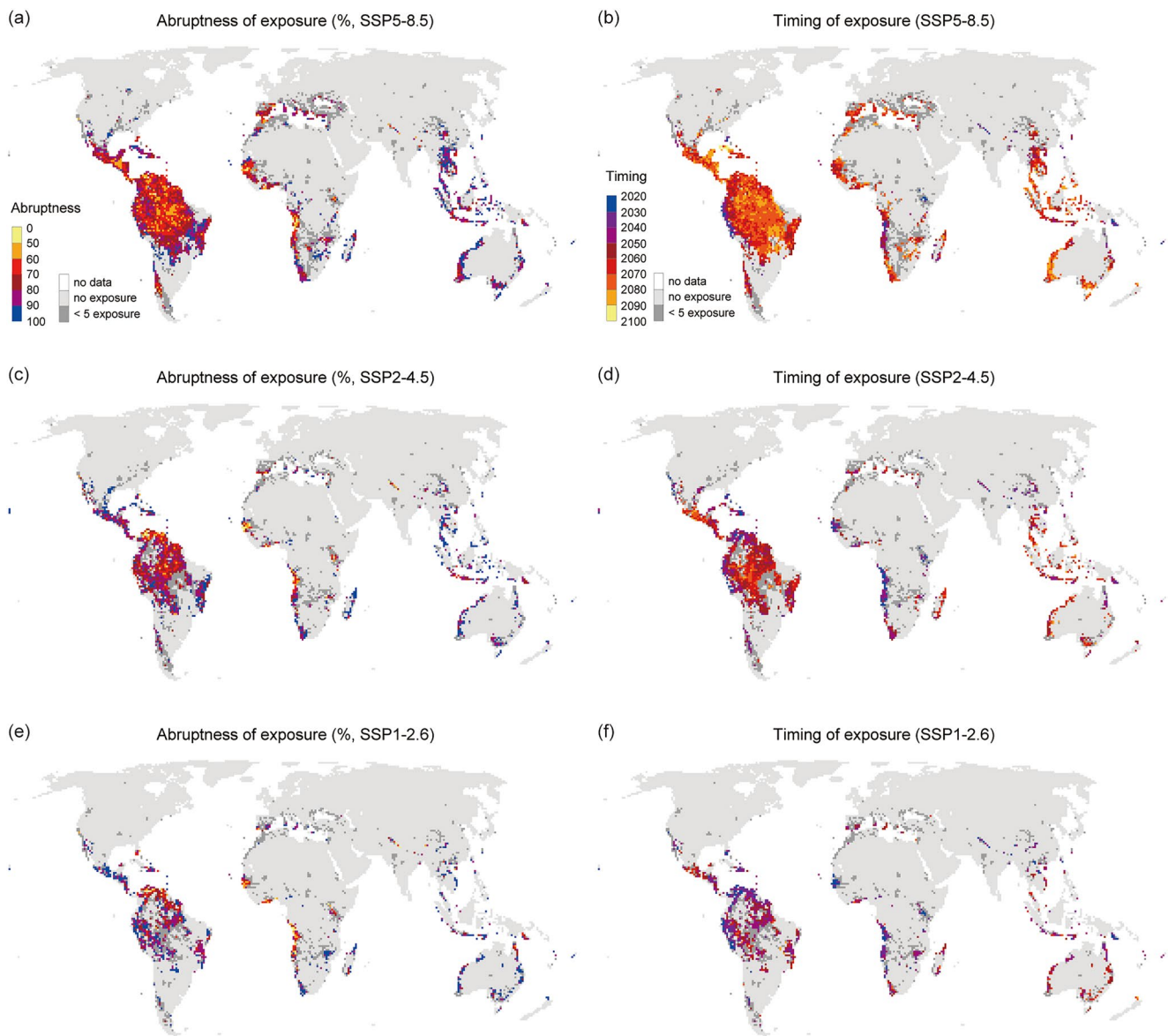
**Figure 2.** Spatial distribution of abruptness and timing of exposure for local assemblage. (a) Exposure abruptness under the SSP5-8.5 scenario, (b) exposure timing under the SSP5-8.5 scenario, (c) same as (a) but under the SSP2-4.5 scenario, (d) same as (b) but under the SSP2-4.5 scenario, (e) same as (a) but under the SSP1-2.6 scenario, and (f) same as (b) but under the SSP1-2.6 scenario.

The cooccurrence of exposure events within a short period suggests that exposure timing can be well described by either the median/mean of the species' exposure year or the midyear of the decade with maximum exposure. We found that the median exposure timing for all exposed terrestrial assemblages was projected to be 2070 under the SSP5-8.5 scenario (Figures 2b and 3b). This exposure timing is close to the timing estimated using the mean exposure year of the species (global median 2069, Figure S9 in Supporting Information S1) and the midyear of the decade with the maximum exposure (global median 2067). Note that the exposure timing varies across different assemblages, and most of the exposure timings for assemblages are found to be later than 2060. Some regions, such as the Andes Mountains and Amazon rainforest, have already encountered this process. After 2060, exposure to unprecedented aridity conditions is projected to spread rapidly across South America (Figures 2b, 2d, and 2f). In most previous studies, the abruptness of exposure has not been reported. They usually suggest a more gradual increase in biodiversity loss and species extinctions driven by climate change (Newbold, 2018; Warren et al., 2018). This gradual increase in the risk of biodiversity loss might result from the aggregation of global assemblages, which smooths out the difference in abrupt exposure timing across local assemblages. Although
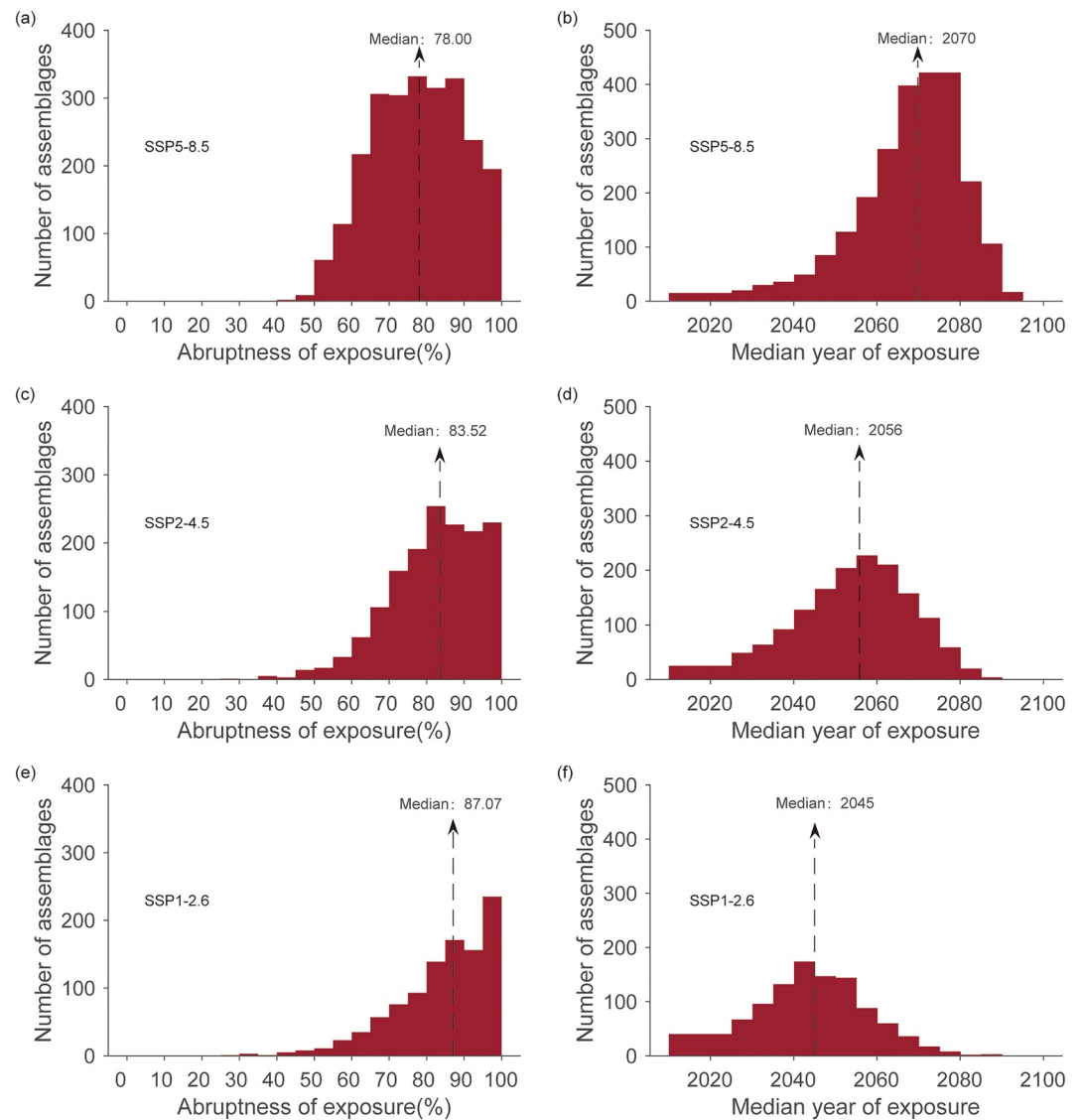
**Figure 3.** Histograms of abruptness and timing of exposure for local assemblage. (a) Exposure abruptness under the SSP5-8.5 scenario, (b) exposure timing under the SSP5-8.5 scenario, (c) same as (a) but under the SSP2-4.5 scenario, (d) same as (b) but under the SSP2-4.5 scenario, (e) same as (a) but under the SSP1-2.6 scenario, and (f) same as (b) but under the SSP1-2.6 scenario.

global aggregation can provide insights into the mitigation of the SSP5-8.5 to SSP2-4.5 (SSP1-2.6) emissions scenario in reducing the exposure magnitude by 6.91% (10.12%) and delaying the onset of exposure by 30 (43) years (Figure 1a), it is likely to overlook the abrupt nature of exposure and risk of ecological disruption within local assemblages and regional hotspots (Table 2).

### 3.3. Hotspots of Local Exposure

The shape of the horizon profiles, including the magnitude, abruptness, and time of local exposure, and the potential risk of ecological disruption were found to vary significantly across the globe (Figures 1c–1e). Although the exposure magnitude aggregated from all terrestrial assemblages showed a smooth, gradual increase in the risk of biodiversity loss (Figure 1a), the situation is projected to be much more dramatic in local hotspot areas (Figure 1c), which is very likely to result in potential abrupt disruptions within local assemblages. Because the averaging effect at the hotspot local scale can considerably smooth the abruptness and timing of exposure during the aggregation of results from multiple GCMs, here, we illustrate the horizon profiles for one selected

**Table 2**
*Averages (Median and Mean) of the Abruptness and Timing of Exposure for Terrestrial Vertebrate Species Under the SSP5-8.5, SSP2-4.5, and SSP1-2.6 Scenarios*

| | | | All terrestrial vertebrate | Amphibian | Mammal | Bird | Reptile |
|---|---|---|---|---|---|---|---|
| SSP5-8.5 | Abruptness (%) | Median | 78.00 | 76.72 | 78.13 | 76.48 | 80.70 |
| | | Mean | 77.78 | 77.25 | 77.88 | 76.78 | 80.56 |
| | Timing | Median | 2070 | 2069 | 2072 | 2072 | 2072 |
| | | Mean | 2068 | 2067 | 2070 | 2070 | 2071 |
| SSP2-4.5 | Abruptness (%) | Median | 83.52 | 86.74 | 85.42 | 82.19 | 90.56 |
| | | Mean | 82.13 | 85.70 | 84.43 | 81.04 | 88.91 |
| | Timing | Median | 2056 | 2056 | 2054 | 2053 | 2058 |
| | | Mean | 2055 | 2056 | 2054 | 2052 | 2058 |
| SSP1-2.6 | Abruptness (%) | Median | 87.07 | 92.31 | 87.50 | 84.22 | 94.44 |
| | | Mean | 84.41 | 89.26 | 85.56 | 81.75 | 93.29 |
| | Timing | Median | 2045 | 2046 | 2043 | 2042 | 2053 |
| | | Mean | 2046 | 2047 | 2044 | 2042 | 2053 |

GCM (IPSL-CM6A-LR), which yields a moderate exposure level among all GCMs (Figure 4 and Table 3). The horizon profiles of exposure hotspots for the other GCMs are shown in Figure S10 and Table S5 in Supporting Information S1.

According to the projections, the hotspots are projected to be located in current semiarid and even humid regions, most of which are populated with rich species and will experience a significant increase in aridity in the future (Figure S11 in Supporting Information S1). Low-latitude regions such as the southern Mexico and the northern Amazon rainforest are distinctive hotspots projected to be exposed to unprecedented aridity conditions. As humid regions are inhabited by a large number of vertebrate species (Figure S11a in Supporting Information S1), their future aridity conditions are projected to become dryer rapidly and become semiarid regions (AI < 0.5, Figures 4a and 4b). Consequently, tropical terrestrial vertebrate species in these regions will experience abrupt exposure events as the aridity exceeds their realized niche limits. The results show that in the southern Mexico,
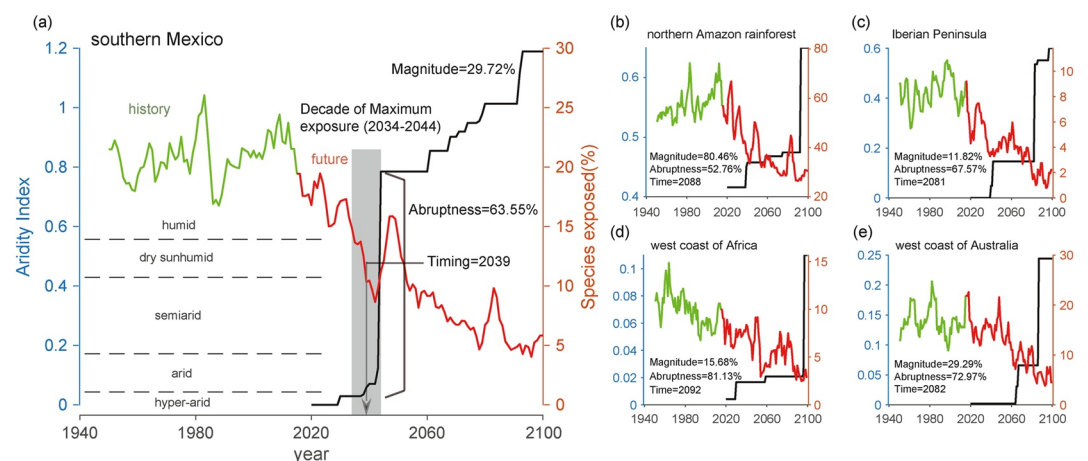


**Figure 4.** Horizon profiles of exposure hotspots driven by future increasing aridity. Horizon profiles (solid black lines) show the mean percentage of geographic range exposure (MPGE) till the end of the century, aggregated from hotspot assemblages exposed to future dryer conditions (solid red lines) beyond species' realized aridity niches calculated from the historical aridity condition (solid green lines). The horizon profiles and aridity trends are shown for a single run of the IPSL-CM6A-LR climate model under the RCP5-8.5 scenario. Note that the timing of exposure is marked using the midyear of the decade with maximum exposure for better demonstration. (a) The southern Mexico, (b) the northern Amazon rainforest, (c) the Iberian Peninsula, (d) the west coast of Africa, and (e) the west coast of Australia.

**Table 3**
*Summary of Local Exposure in Hotspot Regions by 2100 Under the SSP5-8.5 Scenario*

| Hotspots | Magnitude (%) | Abruptness (%) | Timing |
|---|---|---|---|
| South Mexico (A) | 29.72 | 63.55 | 2039 |
| North Amazon rainforest (B) | 80.46 | 52.76 | 2088 |
| Iberian Peninsula (C) | 11.82 | 67.57 | 2081 |
| West coast of Africa (D) | 15.68 | 81.13 | 2092 |
| West coast of Australia (E) | 29.29 | 72.97 | 2082 |

*Note.* The exposure results in the table represent a single run of the IPSL-CM6A-LR climate model. The results for other GCMs are shown in Figure S10 and Table S5 in Supporting Information S1.

abrupt exposure in this region is projected to occur during 2034–2044 under the SSP5-8.5 scenario, with an abruptness of 63.55% and a timing of 2039. By the end of the century, the magnitude is expected to reach 29.72%, meaning that more than one quarter of local vertebrate species will have to live in dryer environments beyond their realized niche limits. The northern Amazon rainforest (Figure 4b) will experience more severe biodiversity loss, threatened by future increasing aridity conditions. The magnitude is projected to reach 80.46% by 2100. The cooccurring species are likely to be exposed to dryer conditions simultaneously in 2088, with an abruptness of 52.76%, leading to devastating ecological disruption in the Amazon rainforest. Other exposure hotspots, such as the Iberian Peninsula (Figure 4c), the west coast of Africa (Figure 4d), and the west coast of Australia (Figure 4e), will experience considerable increases in local aridity conditions, transforming from semiarid to arid and even hyperarid subtypes by 2100. A notable abruptness of exposure has been projected within these areas, resulting in the risk of sudden disruption to local ecosystems and their capacity to maintain current biodiversity. However, in the current arid and hyperarid regions where local species have already adapted to arid environments, such as the west coast of Africa (Figure 4d) and the west coast of Australia (Figure 4e), future increases in aridity can still lead to abrupt exposures at the end of the 21st century and pose a devastating threat to fragile ecosystem functioning.

## 4. Discussion

The global terrestrial surface is predicted to become drier in most emission scenarios (Huang et al., 2016), which greatly threatens the survival of terrestrial species. In this study, we attempted to predict the spatiotemporal dynamics of future vertebrate biodiversity loss driven by the increase in aridity under low-, intermediate-, and high-emissions scenarios using the assessment framework recently proposed by Trisos et al. (2020). Climate simulations from eight selected CMIP6 GCMs were used to estimate the aridity niche limits of the species, construct horizon profiles, and assess the magnitude and abruptness of species exposure. We found that more than 24% of terrestrial assemblages will be exposed to unprecedented aridity conditions beyond their realized niche limits under the high-emissions scenario (Figures 1 and 2). These exposed assemblages were mainly located in low-latitude regions where rich species are populated (Figures 1c and 4, and Figure S11 in Supporting Information S1). Consequently, 55.29% of the species experienced local habitat loss (Table 1). If we successfully managed to reduce the emissions level to the intermediate (SSP2-4.5) and low (SSP1-2.6) scenarios, the onset of abrupt exposure could be delayed by 30 and 43 years, buying valuable time for species to adapt to a dryer environment and mitigate ecological disruption. In addition to the ensemble mean results of the eight selected GCMs, we quantified the spatial uncertainty (standard deviation) of the four exposure indicators across multiple GCMs (Figure S12 in Supporting Information S1). Greater uncertainties of exposure magnitude and exposure number were mainly found in the northern Amazon rainforest (Figures S12a and S12b in Supporting Information S1), where aridity conditions are projected to increase dramatically until the end of the century (Figure S10b in Supporting Information S1). This is mainly because of the larger variances of climate variables (precipitation, temperature, specific humidity, wind speed, surface air pressure, and heat fluxes) in these regions across multiple GCMs, which leads to disparities in local exposure identification. Regarding exposure abruptness and timing, the uncertainties across multiple GCMs do not exhibit a particular spatial heterogeneity (Figures S12c and S12d in Supporting Information S1).

Trisos et al. (2020) used temperature, and precipitation projections from multiple General Circulation and Earth System Models developed for CMIP5 to predict future biodiversity loss spatiotemporal dynamics. Compared with the species exposed to the unprecedented temperature rise in the study by Trisos et al. (2020), the magnitude and geographical range of exposure to future aridity increase in our results are relatively smaller. Most assemblages exposed to aridity increase fall within the geographical range of exposure to temperature rise, except for a few, such as the west coast of Australia and the western cape of South Africa. This is probably because AI is a more synthetic indicator; thus, the future trend of aridity is determined by multiple climate variables, such as temperature, precipitation, surface evaporation, and transpiration (Milly & Dunne, 2016; Yang et al., 2019). Nevertheless, most hotspots exposed to unprecedented aridity conditions geographically overlap, with a higher magnitude of exposure driven by temperature increase. For example, regions of western Mexico, the Amazon rainforest, and

Southeast Asia are heavily exposed to both increasing aridity and rising temperatures (Figure 1). Threatened species living in these areas, such as *Ateles belzebuth*, *Plectrohyla sagorum*, and *Macaca nigra*, face challenges, as they are sensitive to changes in temperature and aridity. Although the magnitude of exposure to aridity increase is smaller than that to temperature rise, abruptness is relatively higher globally (78% for aridity increase vs. 61% for temperature warming). This suggests a higher percentage of exposed species occurring within the decade of maximum exposure in the assemblages, especially for the exposed regions in Southeast Asia (dark blue assemblages in Figures 2a, 2c, and 2e). It is worth noting that the timings of abruptness for the Amazon rainforest in this study (2060–2080 under the SSP5-8.5 scenario, Figure 2) are very close to those assessed by the unprecedented temperature rise in Trisos et al. (2020). This suggests that a large proportion of species in the Amazon rainforest will be exposed to both increasing aridity and rising temperatures simultaneously or temporally adjacent within the same decade from 2060 to 2080. Thus, the magnitude and abruptness of local exposure and the timing of this exposure may be underestimated to a certain extent because our results do not consider risks introduced to the joint threats from local warming and drought events. We caution that the concurrent extremes of increasing aridity and rising temperature may amplify the exposure risks and lead to more compounded biodiversity loss (Masson-Delmotte et al., 2021), resulting in a greater potential for sudden disruption to local ecosystems and the services they provide.

Given that AI is an indicator that focuses more on the average dryness of the land surface for a longer time (Greve et al., 2019; Xu et al., 2021), we used the annual AI to approximate the climate conditions. However, vertebrate species may be sensitive to extremely dry environments during a shorter time, that is, monthly intervals. Thus, we also conducted the analysis procedure using the AI of the driest month in each year, including the determination of ecological niches of species and generation of the horizon profiles. The results show that (Figure S13 in Supporting Information S1, a single run of the IPSL-CM6A-LR model under the SSP5-8.5 scenario), the hotspots of exposure (magnitude, abruptness, timing, and the number of exposures) were distributed similarly to the global picture between results using annual and monthly aridity indices. The geographic range of exposure was slightly smaller when we used the AI of the driest month, but more severe exposure was observed in some regions of southeast Australia and southern Africa. However, the calculation of AI for the driest month and the exposure assessment may inherit substantial uncertainties because the monthly climate data in CMIP6-GCMs are not always complete throughout every year for the variables required to calculate the monthly PET. We will continue to conduct this investigation in the future when more climate data are available. Additionally, the assessment of exposure to unprecedented aridity conditions can be conducted using other aridity indices that account for both surface water supply and evaporative demand, for example, the De Martonne AI and the standardized precipitation evapotranspiration index. Although the exposure magnitude and its spatial pattern may vary using these alternative aridity indices, we do not expect significant differences in the hotspot regions and exposure abruptness, considering that the aridity conditions and their trends quantitated using these indices are usually well correlated with each other (Moral et al., 2016; Salamon-Albert et al., 2016; Speich, 2019).

Note that the exposure to the unprecedented aridity condition in this study may not necessarily cause extinction but only provides a precautionary warning for biodiversity risk. This is mainly because of the following considerations and sources of uncertainty. First, owing to the lack of actual physiological niche data for all terrestrial vertebrate species, we used the local aridity condition during the historical period (1950–2014) to calculate the species' niche limit. Therefore, the niche limit calculated in this manner is realized instead of the true limit to persistence, which may underestimate the tolerance of species to the dryer environment, considering that the species may not have reached its actual physiological limits during 1950–2014. Second, we performed outlier removal in calculating the realized aridity limit of the species to avoid extreme values in the time-series AI values calculated from individual GCM at some ecological assemblages. These preprocesses of outlier removal may accidently remove AI values within the aridity niche. Consequently, the calculated tolerance of species to aridity conditions may be potentially underestimated, leading to an overestimation of the negative effects threatened by the future increasing aridity conditions. Third, we identified the local exposure at the assemblages without considering the potential for species' immigration to more humid regions or physiological adaptation to the dryer environment; however, local habitat losses are inevitable.

In this analysis, we calculated the species-realized niche limits and performed exposure assessments at a spatial resolution of 100 km. This resolution was chosen to maintain consistency with the grain size of the EOO map of species, considering that a grain size of 100 km is a favorable balance between maintaining spatial details and avoiding overestimating species richness and distributions (Hurlbert & Jetz, 2007; Jetz et al., 2008). However,

grids at such coarse resolution may contain spatial climate heterogeneity and thus may potentially underestimate the range of the species niche, leading to an overestimation of the abruptness of exposure. We quantified the spatial climate heterogeneity (range of AI at each 100 km) with historical (1970–2000) AI data available at ~1 km resolution (Zomer et al., 2022) and then performed a preliminary test to determine whether the abruptness of horizon profiles is related to the spatial heterogeneity of AI. We found that assemblages with higher spatial climate heterogeneity (range of AI > fourth quantile, gray bars in Figure S14 in Supporting Information S1) exhibited similar exposure profiles to those with lower climate heterogeneity (range of AI < first quantile, red bars in Figure S14 in Supporting Information S1). This suggests that the exposed assemblages with high spatial climate heterogeneity can still be identified well, even though the analyses were conducted at a coarse resolution of 100 km. Although the use of finer-scale data may lead to a slightly different abruptness of exposure across assemblages, the key conclusion that assemblage exposure to future unprecedented aridity conditions occurs abruptly would not change. Nevertheless, the analyses based on coarse grid units may likely result in the overestimation of the exposure risk because, in reality, species can still find climate refugia at finer scales within assemblages with high climate heterogeneity.

Another limitation of this study is that we only considered the direct threats of increasing aridity to the biodiversity loss of vertebrate species. The increase in aridity has overwhelmingly detrimental impacts on the survival and growth of vegetation across local ecosystems that provide critical habitat resources (e.g., food, shelter, and breeding sites) for vertebrate species. For example, some previous studies have suggested that changes in aridity would degrade tropical forest canopies (Brawn et al., 2017), increase tree mortality rates (Brawn et al., 2017; Hilker et al., 2014; McDowell et al., 2018), and reduce gross primary production in the ecosystem (Piao et al., 2019), thereby decreasing the abundance and population growth of local species (Aguirre-Gutierrez et al., 2020; Hilker et al., 2014). Thus, without considering the indirect effects mediated through changes in local vegetation, our assessment may underestimate the magnitude and abruptness of exposure to future increases in aridity. In addition, we only focused on species exposure to future increases in aridity, which probably leads to more frequent drought events. However, the opposite trend of future aridity change, a decrease in aridity and wetter conditions in specific regions, may also affect the survival of some terrestrial vertebrate species. In future studies, we will continue to examine biodiversity losses threatened by this opposite trend of aridity change.

## 5. Conclusions

In this study, we predicted the future temporal dynamics of biodiversity loss among terrestrial vertebrate species driven by increasing aridity at the assemblage scale under three core sets of emission scenarios: SSP1-2.6 (low emissions), SSP2-4.5(intermediate emissions), and SSP5-8.5 (high emissions). We found that, under the SSP5-8.5 scenario, more than 24% of global terrestrial assemblages are projected to have at least one local vertebrate species exposed to unprecedented aridity conditions by 2100, leading to the consequence that ~55% of terrestrial vertebrate species will experience local habitat loss. By the end of the century, the mean magnitude of global exposure had reached 17.47%. More importantly, an average of 78% of exposure abruptness is projected across the exposed terrestrial assemblages, and most of these abrupt exposure events are expected to occur intensively after 2050. Although the magnitude of global average exposure shows a smooth gradual increase in the risk of biodiversity loss, local disruption of terrestrial assemblages is expected to occur because most species within the assemblage are projected to be simultaneously exposed to dryer environments beyond their realized niche limits. Species of amphibian and reptile clades were more sensitive to the increase in aridity, with greater exposure magnitude, abruptness, and local habitat loss than mammal and bird clades species. We also found that if we manage to reduce GHG emissions to the SSP2-4.5 (SSP1-2.6) scenario, the magnitude of exposure can significantly decrease to ~10% (7%) and delay the onset of exposure by 30 (43) years, averaging approximately 14% (30%) of vertebrate species from losing habitat. The derived temporal dynamic of exposure to future increasing aridity provides a precautionary warning of future biodiversity loss and its potential risk of abrupt ecological disruption. Our results also highlight that the decrease and delay of such exposure can be achieved across most terrestrial assemblages by reducing massive GHG emissions. In addition, we caution that the concurrent extremes of increasing aridity and rising temperature in Southeast Asia and Amazon rainforests may amplify exposure risks and lead to more compounded biodiversity loss. Hopefully, these findings can motivate decision-makers to respond early and effectively to future aridity declines, buy valuable time for species to adapt to a dryer environment, and mitigate ecological disruption.

## Conflict of Interest

The authors declare no conflicts of interest relevant to this study.

## Data Availability Statement

The data used in this study were collected from the following sources: the IUCN Red List data set is available from https://www.iucnredlist.org/resources/spatial-data-download, climate change projections of eight selected CMIP6-GCMs are available from https://esgf-node.llnl.gov/projects/cmip6/, and the $CO_2$ concentration data are available from https://greenhousegases.science.unimelb.edu.au/. The assessment results of this study are available at https://doi.org/10.6084/m9.figshare.20787616.

## References

Aadhar, S., & Mishra, V. (2019). A substantial rise in the area and population affected by dryness in South Asia under 1.5°C, 2.0°C and 2.5°C warmer worlds. *Environmental Research Letters*, *14*(11), 114021. https://doi.org/10.1088/1748-9326/ab4862

Aadhar, S., & Mishra, V. (2020). Increased drought risk in South Asia under warming climate: Implications of uncertainty in potential evapotranspiration estimates. *Journal of Hydrometeorology*, *21*(12), 2979–2996. https://doi.org/10.1175/jhm-d-19-0224.1

Aguirre-Gutierrez, J., Malhi, Y., Lewis, S. L., Fauset, S., Adu-Bredu, S., Affum-Baffoe, K., et al. (2020). Long-term droughts may drive drier tropical forests towards increased functional, taxonomic and phylogenetic homogeneity. *Nature Communications*, *11*(1), 3346. https://doi.org/10.1038/s41467-020-16973-4

Allen, R. G., Pereira, L. S., Raes, D., & Smith, M. (1998). *Crop evapotranspiration—Guidelines for computing crop water requirements—FAO Irrigation and drainage paper 56* (300 pp.). FAO.

Bay, R. A., Rose, N. H., Logan, C. A., & Palumbi, S. R. (2017). Genomic models predict successful coral adaptation if future ocean warming rates are reduced. *Science Advances*, *3*(11), e1701413. https://doi.org/10.1126/sciadv.1701413

Bellard, C., Bertelsmeier, C., Leadley, P., Thuiller, W., & Courchamp, F. (2012). Impacts of climate change on the future of biodiversity. *Ecology Letters*, *15*(4), 365–377. https://doi.org/10.1111/j.1461-0248.2011.01736.x

Berdugo, M., Delgado-Baquerizo, M., Soliveres, S., Hernández-Clemente, R., Zhao, Y., Gaitán, J. J., et al. (2020). Global ecosystem thresholds driven by aridity. *Science*, *367*(6479), 787–790. https://doi.org/10.1126/science.aay5958

Berg, A., Findell, K., Lintner, B., Giannini, A., Seneviratne, S. I., van den Hurk, B., et al. (2016). Land–atmosphere feedbacks amplify aridity increase over land under global warming. *Nature Climate Change*, *6*(9), 869–874. https://doi.org/10.1038/nclimate3029

Brawn, J. D., Benson, T. J., Stager, M., Sly, N. D., & Tarwater, C. E. (2017). Impacts of changing rainfall regime on the demography of tropical birds. *Nature Climate Change*, *7*(2), 133–136. https://doi.org/10.1038/nclimate3183

Brondízio, E. S., Settele, J., Díaz, S., & Ngo, H. T. (2019). *Global assessment report on biodiversity and ecosystem services of the Intergovernmental Science-Policy Platform on Biodiversity and Ecosystem Services*. IPBES Secretariat.

Chai, R., Mao, J., Chen, H., Wang, Y., Shi, X., Jin, M., et al. (2021). Human-caused long-term changes in global aridity. *npj Climate and Atmospheric Science*, *4*(1), 65. https://doi.org/10.1038/s41612-021-00223-5

Colwell, R. K., Brehm, G., Cardelus, C. L., Gilman, A. C., & Longino, J. T. (2008). Global warming, elevational range shifts, and lowland biotic attrition in the wet tropics. *Science*, *322*(5899), 258–261. https://doi.org/10.1126/science.1162547

Colwell, R. K., & Rangel, T. F. (2009). Hutchinson's duality: The once and future niche. *Proceedings of the National Academy of Sciences of the United States of America*, *106*(supplement_2), 19651–19658. https://doi.org/10.1073/pnas.0901650106

Dave, V., Pandya, M., & Ghosh, R. (2019). Identification of desertification hot spot using aridity index. *Annals of Arid Zone*, *58*, 39–44.

Delgado-Baquerizo, M., Maestre, F. T., Gallardo, A., Bowker, M. A., Wallenstein, M. D., Quero, J. L., et al. (2013). Decoupling of soil nutrient cycles as a function of aridity in global drylands. *Nature*, *502*(7473), 672–676. https://doi.org/10.1038/nature12670

Deutsch, C. A., Tewksbury, J. J., Huey, R. B., Sheldon, K. S., Ghalambor, C. K., Haak, D. C., & Martin, P. R. (2008). Impacts of climate warming on terrestrial ectotherms across latitude. *Proceedings of the National Academy of Sciences of the United States of America*, *105*(18), 6668–6672. https://doi.org/10.1073/pnas.0709472105

Díaz, S., Settele, J., Brondízio, E. S., Ngo, H. T., Agard, J., Arneth, A., et al. (2019). Pervasive human-driven decline of life on Earth points to the need for transformative change. *Science*, *366*(6471), eaax3100. https://doi.org/10.1126/science.aax3100

Elith, J., Graham, H., Anderson, C. P. R., Dudík, M., Ferrier, S., Guisan, A., et al. (2006). Novel methods improve prediction of species' distributions from occurrence data. *Ecography*, *29*(2), 129–151. https://doi.org/10.1111/j.2006.0906-7590.04596.x

Elith, J., & Leathwick, J. R. (2009). Species distribution models: Ecological explanation and prediction across space and time. *Annual Review of Ecology, Evolution, and Systematics*, *40*(1), 677–697. https://doi.org/10.1146/annurev.ecolsys.110308.120159

Feng, S., & Fu, Q. (2013). Expansion of global drylands under a warming climate. *Atmospheric Chemistry and Physics*, *13*(19), 10081–10094. https://doi.org/10.5194/acp-13-10081-2013

García-Palacios, P., Gross, N., Gaitán, J., & Maestre, F. T. (2018). Climate mediates the biodiversity–ecosystem stability relationship globally. *Proceedings of the National Academy of Sciences of the United States of America*, *115*(33), 8400–8405. https://doi.org/10.1073/pnas.1800425115

Gibson, L., Lee, T. M., Koh, L. P., Brook, B. W., Gardner, T. A., Barlow, J., et al. (2011). Primary forests are irreplaceable for sustaining tropical biodiversity. *Nature*, *478*(7369), 378–381. https://doi.org/10.1038/nature10425

Greve, P., Roderick, M. L., Ukkola, A. M., & Wada, Y. (2019). The aridity index under global warming. *Environmental Research Letters*, *14*(12), 124006. https://doi.org/10.1088/1748-9326/ab5046

Hijmans, R. J., Cameron, S. E., Parra, J. L., Jones, P. G., & Jarvis, A. (2005). Very high resolution interpolated climate surfaces for global land areas. *International Journal of Climatology*, *25*(15), 1965–1978. https://doi.org/10.1002/joc.1276

Hilker, T., Lyapustin, A. I., Tucker, C. J., Hall, F. G., Myneni, R. B., Wang, Y., et al. (2014). Vegetation dynamics and rainfall sensitivity of the Amazon. *Proceedings of the National Academy of Sciences of the United States of America*, *111*(45), 16041–16046. https://doi.org/10.1073/pnas.1404870111

Hooper, D. U., Adair, E. C., Cardinale, B. J., Byrnes, J. E. K., Hungate, B. A., Matulich, K. L., et al. (2012). A global synthesis reveals biodiversity loss as a major driver of ecosystem change. *Nature*, *486*(7401), 105–108. https://doi.org/10.1038/nature11118

Huang, J., Yu, H., Guan, X., Wang, G., & Guo, R. (2016). Accelerated dryland expansion under climate change. *Nature Climate Change*, *6*(2), 166–171. https://doi.org/10.1038/nclimate2837

Hurlbert, A. H., & Jetz, W. (2007). Species richness, hotspots, and the scale dependence of range maps in ecology and conservation. *Proceedings of the National Academy of Sciences of the United States of America*, *104*(33), 13384–13389. https://doi.org/10.1073/pnas.0704469104

IPBES. (2019). Summary for policymakers. In S. Díaz, J. Settele, E. S. Brondízio, & H. T. Ngo (Eds.), *Global assessment report on biodiversity and ecosystem services of the Intergovernmental Science-Policy Platform on Biodiversity and Ecosystem Services* (p. 56). IPBES Secretariat.

IPCC. (2021). Climate change 2021: The physical science basis. In V. Masson-Delmotte, et al. (Eds.), *Contribution of Working Group I to the sixth assessment report of the Intergovernmental Panel on Climate Change*. Cambridge University Press.

Jetz, W., Sekercioglu, C. H., & Watson, J. E. (2008). Ecological correlates and conservation implications of overestimating species geographic ranges. *Conservation Biology*, *22*(1), 110–119. https://doi.org/10.1111/j.1523-1739.2007.00847.x

Joppa, L. N., Butchart, S. H. M., Hoffmann, M., Bachman, S. P., Akçakaya, H. R., Moat, J. F., et al. (2016). Impact of alternative metrics on estimates of extent of occurrence for extinction risk assessment. *Conservation Biology*, *30*(2), 362–370. https://doi.org/10.1111/cobi.12591

Li, F., Chung, N., Bae, M.-J., Kwon, Y.-S., Kwon, T.-S., & Park, Y.-S. (2013). Temperature change and macroinvertebrate biodiversity: Assessments of organism vulnerability and potential distributions. *Climatic Change*, *119*(2), 421–434. https://doi.org/10.1007/s10584-013-0720-9

Maclean, I. M. D., & Wilson, R. J. (2011). Recent ecological responses to climate change support predictions of high extinction risk. *Proceedings of the National Academy of Sciences of the United States of America*, *108*(30), 12337–12342. https://doi.org/10.1073/pnas.1017352108

Maestre, F. T., Eldridge, D. J., Soliveres, S., Kéfi, S., Delgado-Baquerizo, M., Bowker, M. A., et al. (2016). Structure and functioning of dryland ecosystems in a changing world. *Annual Review of Ecology, Evolution, and Systematics*, *47*(1), 215–237. https://doi.org/10.1146/annurev-ecolsys-121415-032311

Maidment, D. R. (1993). *Handbook of hydrology*. McGraw-Hill.

Marmion, M., Parviainen, M., Luoto, M., Heikkinen, R. K., & Thuiller, W. (2009). Evaluation of consensus methods in predictive species distribution modelling. *Diversity and Distributions*, *15*(1), 59–69. https://doi.org/10.1111/j.1472-4642.2008.00491.x

Masson-Delmotte, V., Zhai, P., Pirani, A., Connors, S. L., Péan, C., Berger, S., et al. (2021). Climate change 2021: The physical science basis.

McDowell, N., Allen, C. D., Anderson-Teixeira, K., Brando, P., Brienen, R., Chambers, J., et al. (2018). Drivers and mechanisms of tree mortality in moist tropical forests. *New Phytologist*, *219*(3), 851–869. https://doi.org/10.1111/nph.15027

Meinshausen, M., Nicholls, Z. R. J., Lewis, J., Gidden, M. J., Vogel, E., Freund, M., et al. (2020). The shared socio-economic pathway (SSP) greenhouse gas concentrations and their extensions to 2500. *Geoscientific Model Development*, *13*(8), 3571–3605. https://doi.org/10.5194/gmd-13-3571-2020

Meinshausen, M., Vogel, E., Nauels, A., Lorbacher, K., Meinshausen, N., Etheridge, D. M., et al. (2017). Historical greenhouse gas concentrations for climate modelling (CMIP6). *Geoscientific Model Development*, *10*(5), 2057–2116. https://doi.org/10.5194/gmd-10-2057-2017

Middleton, N., & Thomas, D. (1992). *World atlas of desertification, 1992: United Nations Environment Programme (UNEP)*. Edward Arnold.

Milly, P. C., & Dunne, K. A. (2016). Potential evapotranspiration and continental drying. *Nature Climate Change*, *6*(10), 946–949. https://doi.org/10.1038/nclimate3046

Moral, F. J., Rebollo, F. J., Paniagua, L. L., Garcia-Martin, A., & Honorio, F. (2016). Spatial distribution and comparison of aridity indices in Extremadura, southwestern Spain. *Theoretical and Applied Climatology*, *126*(3–4), 801–814. https://doi.org/10.1007/s00704-015-1615-7

Mortimore, M., Anderson, S., Cotula, L., Davies, J., Faccer, K., Hesse, C., et al. (2009). Dryland opportunities: A new paradigm for people, ecosystems and development. In *International Union for Conservation of Nature (IUCN)*.

Newbold, T. (2018). Future effects of climate and land-use change on terrestrial vertebrate community diversity under different scenarios. *Proceedings of the Royal Society B: Biological Sciences*, *285*(1881), 20180792. https://doi.org/10.1098/rspb.2018.0792

Newbold, T., Hudson, L. N., Arnell, A. P., Contu, S., De Palma, A., Ferrier, S., et al. (2016). Has land use pushed terrestrial biodiversity beyond the planetary boundary? A global assessment. *Science*, *353*(6296), 288–291. https://doi.org/10.1126/science.aaf2201

Pendergrass, A. G., & Hartmann, D. L. (2014). The atmospheric energy constraint on global-mean precipitation change. *Journal of Climate*, *27*(2), 757–768. https://doi.org/10.1175/jcli-d-13-00163.1

Penman, H. L. (1948). Natural evaporation from open water, bare soil and grass. *Proceedings of the Royal Society of London. Series A: Mathematical and Physical Sciences*, *193*, 120–145.

Piao, S. L., Zhang, X. P., Chen, A. P., Liu, Q., Lian, X., Wang, X. H., et al. (2019). The impacts of climate extremes on the terrestrial carbon cycle: A review. *Science China Earth Sciences*, *62*(10), 1551–1563. https://doi.org/10.1007/s11430-018-9363-5

Prideaux, G. J., Ayliffe, L. K., DeSantis, L. R. G., Schubert, B. W., Murray, P. F., Gagan, M. K., & Cerling, T. E. (2009). Extinction implications of a chenopod browse diet for a giant Pleistocene kangaroo. *Proceedings of the National Academy of Sciences of the United States of America*, *106*(28), 11646–11650. https://doi.org/10.1073/pnas.0900956106

Román-Palacios, C., & Wiens, J. J. (2020). Recent responses to climate change reveal the drivers of species extinction and survival. *Proceedings of the National Academy of Sciences of the United States of America*, *117*(8), 4211–4217. https://doi.org/10.1073/pnas.1913007117

Salamon-Albert, E., Lorincz, P., Pauler, G., Bartha, D., & Horvath, F. (2016). Drought stress distribution responses of continental Beech forests at their Xeric Edge in Central Europe. *Forests*, *7*(12), 298. https://doi.org/10.3390/f7120298

Scheffer, M., Bascompte, J., Brock, W. A., Brovkin, V., Carpenter, S. R., Dakos, V., et al. (2009). Early-warning signals for critical transitions. *Nature*, *461*(7260), 53–59. https://doi.org/10.1038/nature08227

Shi, H., Tian, H. Q., Lange, S., Yang, J., Pan, S. F., Fu, B. J., et al. (2021). Terrestrial biodiversity threatened by increasing global aridity velocity under high-level warming. *Proceedings of the National Academy of Sciences of the United States of America*, *118*(36), e2015552118.

Speich, M. J. R. (2019). Quantifying and modeling water availability in temperate forests: A review of drought and aridity indices. *iForest: Biogeosciences and Forestry*, *12*, 1–16. https://doi.org/10.3832/ifor2934-011

Stadler, S. J. (1998). Aridity indices. In *Encyclopedia of hydrology and lakes* (pp. 78–83). Springer Netherlands.

Swann, A. L., Hoffman, F. M., Koven, C. D., & Randerson, J. T. (2016). Plant responses to increasing $CO_2$ reduce estimates of climate impacts on drought severity. *Proceedings of the National Academy of Sciences of the United States of America*, *113*(36), 10019–10024. https://doi.org/10.1073/pnas.1604581113

Tebaldi, C., Debeire, K., Eyring, V., Fischer, E., Fyfe, J., Friedlingstein, P., et al. (2021). Climate model projections from the scenario model Intercomparison Project (ScenarioMIP) of CMIP6. *Earth System Dynamics*, *12*(1), 253–293. https://doi.org/10.5194/esd-12-253-2021

Trisos, C. H., Merow, C., & Pigot, A. L. (2020). The projected timing of abrupt ecological disruption from climate change. *Nature*, *580*(7804), 496–501. https://doi.org/10.1038/s41586-020-2189-9

Urban, M. C. (2015). Accelerating extinction risk from climate change. *Science*, *348*(6234), 571–573. https://doi.org/10.1126/science.aaa4984

Wang, C., Wang, X. B., Liu, D. W., Wu, H. H., Lu, X. T., Fang, Y. T., et al. (2014). Aridity threshold in controlling ecosystem nitrogen cycling in arid and semi-arid grasslands. *Nature Communications*, *5*(1), 4799. https://doi.org/10.1038/ncomms5799

Wang, X., Jiang, D., & Lang, X. (2021). Future changes in aridity index at two and four degrees of global warming above preindustrial levels. *International Journal of Climatology*, *41*(1), 278–294. https://doi.org/10.1002/joc.6620

Warren, R., Price, J., Graham, E., Forstenhaeusler, N., & VanDerWal, J. (2018). The projected effect on insects, vertebrates, and plants of limiting global warming to 1.5°C rather than 2°C. *Science*, *360*(6390), 791–795. https://doi.org/10.1126/science.aar3646

Warren, R., VanDerWal, J., Price, J., Welbergen, J. A., Atkinson, I., Ramirez-Villegas, J., et al. (2013). Quantifying the benefit of early climate change mitigation in avoiding biodiversity loss. *Nature Climate Change*, *3*(7), 678–682. https://doi.org/10.1038/nclimate1887

Wen, M., Cheng, D., Song, J., Zhang, G., Lai, W., & Jiang, W. (2018). Impacts of climate change on aridity index and its spatiotemporal variation in the Loess Plateau of China, from 1961 to 2014. *Environmental Earth Sciences*, *77*(4), 1–12. https://doi.org/10.1007/s12665-018-7304-y

Xu, H.-J., Wang, X.-P., Zhao, C.-Y., Shan, S.-Y., & Guo, J. (2021). Seasonal and aridity influences on the relationships between drought indices and hydrological variables over China. *Weather and Climate Extremes*, *34*, 100393. https://doi.org/10.1016/j.wace.2021.100393

Yang, Y., Roderick, M. L., Zhang, S., McVicar, T. R., & Donohue, R. J. (2019). Hydrologic implications of vegetation response to elevated $CO_2$ in climate projections. *Nature Climate Change*, *9*(1), 44–48. https://doi.org/10.1038/s41558-018-0361-0

Zomer, R. J., Xu, J. C., & Trabucco, A. (2022). Version 3 of the global aridity index and potential evapotranspiration database. *Scientific Data*, *9*(1), 409. https://doi.org/10.1038/s41597-022-01493-1